Ar$^+$-induced mixing mechanisms in metal–metal bilayer systems

S. O. KIM*, J. H. SONG, H. G. JANG, S. S. KIM, J. J. WOO‡, C. N. WHANG
Department of Physics, Yonsei University, Seoul 120-749, Korea

R. J. SMITH
Department of Physics, Montana State University, Bozeman, MT 59717, USA

Ion-beam mixing in Al–Pd, Al–Cr, Pd–Cu, Ag–Cu and Ag–Fe bilayers has been studied using Rutherford backscattering spectroscopy (RBS) and Auger electron spectroscopy (AES) over an ion dose range between 1×10^{15} and 1×10^{16} Ar$^+$ cm^{-2} at room temperature. RBS and AES results show that the mixing efficiency of the light elements is higher than that of the heavy elements. The mixing efficiency of a heavy element is independent of the heat of mixing energy, while that of a light element has a close relation with the heat of mixing. The experimental results are discussed in terms of cascade mixing and thermal spike mixing.

1. Introduction

Irradiation of a solid with energetic ions results not only in the production of vacancies and interstitial atoms, but also in the related phenomenon of ion-beam mixing. This ion-beam mixing process turns out to be a very suitable technique in producing either crystalline or amorphous surface alloys [1]. However, the basic mechanisms of ion-induced mixing are not yet very well understood; the rate of mixing of two component systems under heavy ion bombardment cannot be explained only by the cascade mixing mechanism. In some cases, thermal spike and/or radiation-enhanced diffusion (RED) effects are believed to play an important role. Thus more than one mechanism is operating in a particular system.

Ion-induced mixing processes such as cascade, thermal spike and RED are very closely related to the damage density produced by ion irradiation. The damage density profile due to ion bombardment in a binary system reveals [2] that the damage density in the heavy-element side is higher than that in the light-element side. This difference in the damage density between the light-element and heavy-element sides might affect the atomic transport of the constituents in a binary system during ion-beam mixing. Rauschenbach et al. [3] reported that in the Al–Fe bilayer system the mixing efficiency of Al (light element) is significantly larger than that of Fe (heavy element) because of a strong dependence of diffusion coefficients on the damage profiles. Tao et al. [4] noted that in metal–Si systems the atoms from the low damage-density region (Si layer) move preferentially into the high damage-density region (the metal layer), so the light element (Si atoms) plays the role of the moving species during ion-induced mixing due to damage-controlled atomic motion.

In this study we report the mixing efficiencies of constituents in metal–metal bilayer systems (Al–Pd, Al–Cr, Pd–Cu, Ag–Cu and Ag–Fe). The mixing efficiencies of the constituents in bilayer systems were investigated by Rutherford backscattering spectroscopy (RBS) and Auger electron spectroscopy (AES). The experimental results are interpreted in terms of the cascade mixing and thermal spike-induced mixing mechanisms, associated with the nuclear energy deposition profiles.

2. Experimental procedure

Metal–metal thin-film bilayers were deposited on a single-crystalline Si substrate by electron beam evaporation in a high vacuum (10^{-7} torr). The thickness of the top metal layer (Al, Pd or Ag) was designed to match the mean projected range of the 80 keV Ar$^+$ ions in the top layer. The deposition rate and evaporated thickness of each element were monitored and controlled by a vibrating quartz-crystal deposition monitor. Ion-beam mixing was carried out with 80 keV Ar$^+$ ions at room temperature in a vacuum of 2×10^{-7} torr. To avoid sample heating due to ion bombardment the substrate was glued to a large copper block and ion currents were maintained below 1.5 μA cm^{-2}. The ion fluence ranged between 1×10^{15} and 1.5×10^{16} Ar$^+$ cm^{-2}.

The mixing efficiencies of Al and Pd in the Al–Pd bilayer system were investigated using the AES technique. The 595 scanning Auger microprobe in the MSU Advance Materials Center was operated with a primary electron beam of 3.0 keV. Auger depth profiles were obtained using 1 keV Ar$^+$ ion sputter etching with simultaneous monitoring of the Al

LMM (68 eV) and Pd *MNN* (330 eV) Auger transitions. Intensities of the Auger peaks were determined as the peak-to-peak heights in the derivative spectra ($dN(E)/dE$ mode). The residual pressure and Ar background pressure were in the range of 10^{-9} and 10^{-6} torr, respectively.

The RBS technique was employed to determine the average mixing efficiencies of light and heavy elements in bilayer systems. For this, the target was tilted to an angle of 60° from the incident He^+ beam, and the He^+ beam extracted from a 2 MeV Van de Graaff accelerator [5] was magnetically analysed and collimated to a 1 mm^2 spot on the sample. The energy of the backscattered He^+ ions was analysed with a solid-state detector at a laboratory scattering angle of 160°. The energy resolution of the analysing system was 16 keV.

3. Results and discussion

In order to examine the atomic mixing process in the Al–Pd system during Ar^+ bombardment, we measured AES depth profiles of Al (Fig. 1a) and Pd (Fig. 1b) after mixing, using 5×10^{15} and 1×10^{16} Ar^+ cm^{-2}, along with that of the as-deposited sample. The evaporated film thicknesses of Al (top layer) and Pd (bottom layer) were 70 and 20 nm, respectively. The AES depth profile of the as-deposited sample exhibits a rather sharp transition region at the interface. With increasing Ar^+ ion dose, the profiles tend to become broader across the interface region. This result clearly indicates that intermixing
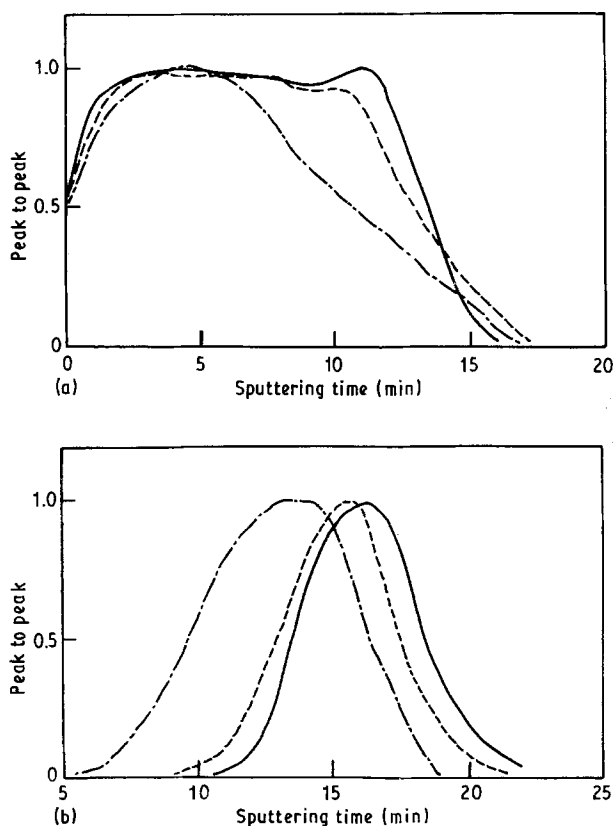
Figure 1 AES depth profiles of (a) Al and (b) Pd in Al–Pd bilayered system for (———) an as-deposited sample, and for ion-beam mixed samples with doses of (———) 5×10^{15} and (—·—) 1×10^{16} Ar^+ cm^{-2}.

has occurred through the Al–Pd interface as a result of Ar^+ bombardment. Also the peak position of the Pd signal moves progressively toward smaller sputtering time with increasing ion dose because of the sputter-removal of Al atoms during ion-beam mixing. The thickness of Al removed by sputtering is 10 nm at a dose of 1×10^{16} cm^{-2}, as determined from the RBS area analysis.

The AES depth profiling method has the advantage that in the case of smooth sputter removal, excellent depth resolution can be obtained, limited only by the escape depth of the Auger electrons ($\simeq$ 1 nm). However, a severe problem arises in determining the sputtered depth since the sputtering rate is generally matrix-dependent. In this case, a depth scale with high accuracy can be obtained by measuring independently the individual thicknesses of the evaporated metal layers. The thicknesses of the evaporated Al and Pd layers are evaluated from the RBS spectra of the as-deposited sample obtained with the sample normal tilted to an angle of 78° from the incident He^+ beam. The RUMP program [6] for the backscattering spectra is employed to evaluate the thickness of the evaporated layers. By assuming that the concentrations at the Al–Pd interface in the as-deposited sample is a step-like function, the sputtering time corresponding to the evaporated film thickness can be defined here as the FWHM of the AES depth profile. Comparing the RBS spectra with the AES depth profile for the as-deposited sample, the ion etching rates for the Al and Pd layers for 1 keV Ar^+ during AES depth-profiling are found to be 5.15 and 5.02 nm min^{-1}, respectively.

In the case of ion-beam mixing experiments, Fick's law is generally used under the assumption that the diffusion coefficient, D, is a constant, i.e. independent of atomic concentration, which results in a Gaussian error function type of depth profile [7] in the interface region. However, this assumption can never be used in a case where the depth profile of the interface deviates from the Gaussian error function as it does for a dose of 1×10^{16} cm^{-2} in Fig. 1. We evaluate the diffusion coefficients or the mixing efficiencies as a function of depth from the AES depth profiles using the Boltzmann–Matano method [8].

In a real experiment, the diffusion coefficients can vary with concentration gradient. In this case, Fick's second law must be written as

$$\frac{\partial c}{\partial t} = \frac{\partial}{\partial x}\left(D\frac{\partial c}{\partial x}\right) \tag{1}$$

where c is the atomic concentration and x is the position along the depth. We assume that the initial conditions for $c(x, t)$ are $c(x > 0, 0) = 1$ and $c(x < 0, 0) = 0$ for the Al layer, and $c(x < 0, 0) = 1$ and $c(x > 0, 0) = 0$ for the Pd layer. For these initial conditions, the partial differential Equation 1 can be transformed into an ordinary homogeneous differential equation for $c(y)$ using the substitution $y = x/t^{1/2}$. Using this definition of y and Equation 1, the relation becomes

$$2D(c')t = -\left(\frac{dx}{dc}\right)_{c'}\int_0^{c'} x\,dc \tag{2}$$

where c' is any concentration $0 < c' < 1$. When we define the mixing efficiency of a bilayer system as $\eta = 4Dt/\phi$ (ϕ is the ion dose), the mixing efficiency for a given concentration c' can be calculated from the slope of dx/dc at $c = c'$ and the area $\int_0^{c'} x\,dc$. To calculate η, the measured depth profile data have been fitted to a smooth cubic spline function, and then the differentiation and integration have been performed.

Fig. 2b shows the calculated mixing efficiencies of Al and Pd for the sample mixed with the dose of $1 \times 10^{16}\,Ar^+\,cm^{-2}$ along with an AES depth profile (Fig. 2a) of the same sample for comparision. This result shows clearly that the mixing efficiencies, i.e. the diffusion coefficients, are far from being constants. The maxima of mixing efficiencies for Al and Pd are found near the Al–Pd interface, and that for Al is located behind the interface, while that for Pd is located in front of the interface. The maximum value of η for Al is significantly higher than that for Pd by a factor of 4. This phenomenon of Al diffusing faster than Pd might be correlated with collisional events such as cascade, thermal spike and RED effects, and different atomic mixing mechanisms between the light element (Al) and heavy element (Pd).

The ion-induced mixing process is commonly divided into three stages [9, 10] according to the time evolution occurring in a given system:

1. During the first $\simeq 10^{-13}$ s, a set of cascades is initiated through individual collisions of moving atoms (primary ions and recoils) with target nuclei at rest (cascade mixing regime).
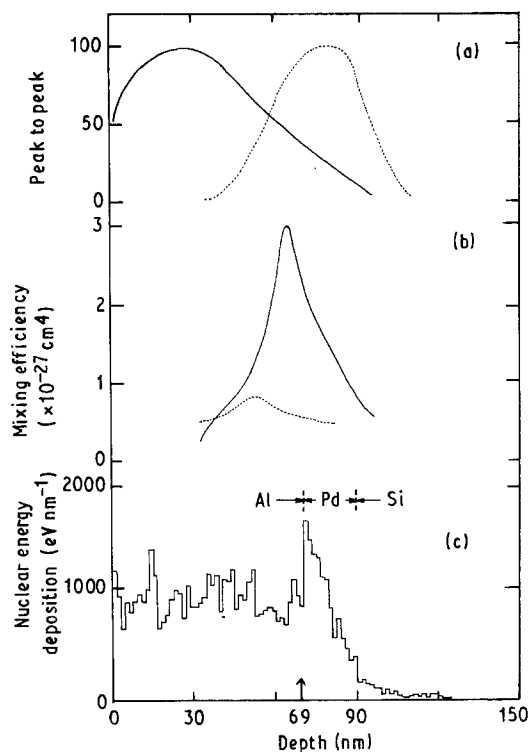
2. If the deposited energy is sufficiently large, the highly disordered cascade region achieves local thermal equilibrium with its surroundings during the first few picoseconds. The resulting local hot region, which may survive for up to $\simeq 10^{-11}$ s, is then called a thermal spike (thermal spike regime).

3. Eventually the atoms in the vicinity of the initial cascade will have reached thermal equilibrium, and return slowly to ambient temperature. Then atomic motion occurs by thermal diffusion of irradiation-induced defects, known as radiation-enhanced diffusion. This type of transport occurs over time intervals of from 10^{-11} s up to more than 1s (RED regime).

All the phases are very closely related to the nuclear energy deposition distribution or the damage density profile produced by ion irradiation. Guinan and Kinney [11] have observed, using molecular dynamics computer simulation for high-energy cascades, that almost all defects are produced in the cascade phase, and that a large number of defects annihilate during the thermal spike phase to result in atomic transport that is more than an order of magnitude greater than that predicted from equilibrium transport theory. Also, Biersack [12] has demonstrated theoretically that in a collision cascade the lighter target atoms always have a larger displacement as compared to that of the heavier atoms in a binary system. We suggest that these observations might be the theoretical support for our experimental observations.

Fig. 2c shows the nuclear energy deposition, S_n, profile due to $80\,keV\,Ar^+$ ions in the Al(70 nm)–Pd(20 nm)–Si system. The S_n profile was obtained employing the TRIM Monte Carlo simulation program [13] with 1000 incident Ar^+ ions. The projected range of Ar^+ ($R_p = 69 \pm 21$ nm) is marked with an arrow. As shown in Fig. 2, the S_n profile is very similar to the depth dependence of the mixing efficiencies: near to the interface, the energy deposition is highest and the mixing efficiencies show maxima, also the energy deposition on the Pd side is higher than on the Al side and the value of η for Al is significantly higher than that of Pd. These results reveal that the phenomenon of Al diffusing faster than Pd relates closely to the nuclear energy deposition profile and its related mixing mechanism.

Therefore we suggest that the higher energy deposition on the Pd side induces a pronounced vacancy concentration, which causes a pronounced increase in diffusion of Al by the RED mechanism via vacancy migration and/or thermal spike-induced mixing [14]. In fact, Al has the lowest vacancy migration energy among metals [15] and a high solubility in Pd (about 18 at %) [16] compared with the negligible one of Pd in Al. Moreover the Al–Pd binary system has a relatively high negative heat of mixing energy ($\Delta H_m = -104\,kJ\,g$-at^{-1}) [16]. As a consequence of the high energy deposition on the Pd side, the low value of migration energy for Al, the high solubility of Al in Pd, and the highly negative value of ΔH_m, radiation-enhanced diffusion and/or thermal spike-induced mixing would be more pronounced for Al than for Pd, and Al atoms may diffuse into the Pd matrix due to a

Figure 2 (a) AES depth profiles of (———) Al and ($\cdots$)Pd at a dose of $1 \times 10^{16}\,Ar^+\,cm^{-2}$. (b) Depth profiles of calculated mixing efficiencies for (———) Al and ($\cdots$) Pd at a dose of $1 \times 10^{16}\,Ar^+\,cm^{-2}$. (c) Depth profile of the nuclear energy deposition, S_n, due to 80 keV Ar^+ in the Al (70 nm)–Pd (20 nm)–Si system.
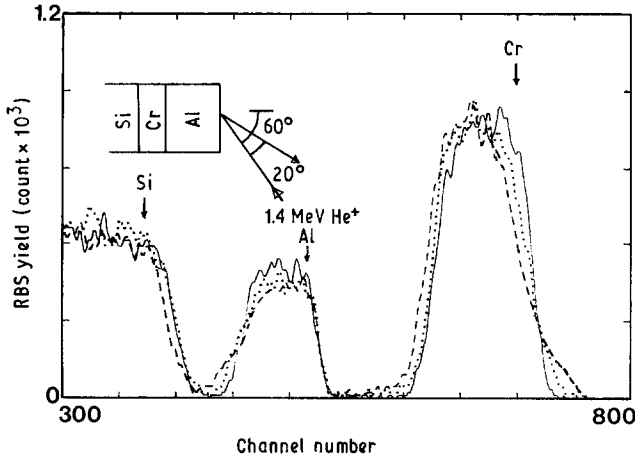
Figure 3 RBS spectra of Al–Cr bilayers for (——) an as-deposited sample and for samples irradiated with doses of (···) 6×10^{15} and (– – –) 9×10^{15} Ar^+ cm^{-2} (1.0 keV per channel).

Figure 4 Atomic mixing variances of (——) Al and (– – –) Cr as a function of ion dose.

different diffusion mechanism from that of the Pd atoms.

In order to elucidate our suggestion in more detail, we investigated the average mixing efficiencies of the light elements and heavy elements in Al–Cr, Pd–Cu, Ag–Cu and Ag–Fe bilayer systems using the RBS technique. Fig. 3 shows typical RBS spectra for Al(70 nm)–Cr(40 nm) bilayers for the as-deposited sample and for samples mixed with doses of 6×10^{15} and 9×10^{15} Ar^+ cm^{-2}. The incident energy of He^+ was 1.4 MeV and the target was tilted to an angle of 60° from the direction of the incident He^+ beam. All the spectra have been normalized to the height of the random Si substrate signal obtained from the as-deposited sample. The signals for various elements are indicated by arrows in the figure. It can be seen from Fig. 3 that Ar^+ ion bombardment has caused broadening of the RBS signal for Cr and Al; the signal portion of the low-energy edge for Al is progressively shifted to lower energy with increasing ion dose, while the high-energy edge for Cr moves to higher energy.

To evaluate the average mixing efficiencies for Al and Cr, the mixing variances of Cr and Al, defined as $\sigma^2 = 2Dt$, are extracted by fitting the high-energy edge of the Cr signal (bottom layer) and the low-energy edge of the Al signal (top layer) in the RBS spectra to an error function, $erf(x/2^{1/2}\sigma)$. The RUMP program [6] is employed to simulate the RBS spectra, taking into account both detector resolution and the energy straggling effect. Fig. 4 shows clearly that the mixing variances increase linearly with ion dose. The mixing efficiencies of Al and Cr, defined as $\eta = d(4Dt)/d\phi$ or $2d(\Delta\sigma^2)/d\phi$, can be evaluated from the slopes of the linear fit. The mixing efficiencies for Al and Cr are found to be 12.6 and 2.38 nm^4, respectively. The value of η for Al is significantly higher than that for Cr as in the case of the Al–Pd system.

Plots of the mixing variance, $\sigma^2 = 2Dt$, versus ion dose have been constructed for the Pd–Cu, Ag–Cu and Ag–Fe bilayer systems. The data points for each system were least-squares fitted with a straight line, and the value of η was evaluated from the slope of the linear fit. Fig. 5 shows the mixing efficiencies of heavy
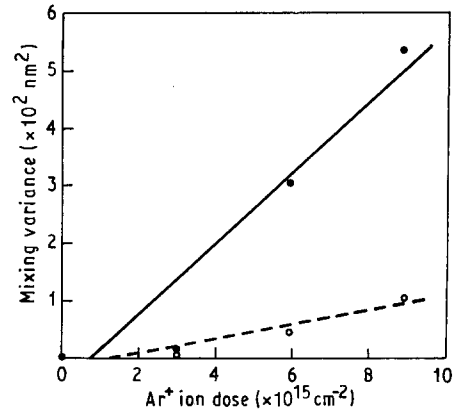
elements, η_H, in binary systems versus ΔH_m (Fig. 5a) and the ratios of the mixing efficiencies of light elements (η_L) to η_H in a binary system as a function of ΔH_m (Fig. 5b). These results show that η_H is independent of ΔH_m, while the value of η_L/η_H reveals a strong dependence on ΔH_m. We present in the following discussion a qualitative analysis for these phenomena in terms of cascade and thermal spike-induced atomic mixing.

Sigmund and Gras-Marti [17] derived an analytic expression for the mixing efficiency, η, in the cascade region:

$$\eta = \frac{2}{3}\Gamma_0 \frac{S_n}{N} \xi_{21} \frac{R_c^2}{E_d} \tag{3}$$

Here $\Gamma_0 = 0.608$, $\xi_{21} = [4M_1M_2/(M_1 + M_2)^2]^{1/2}$, where M_1 and M_2 are the atomic mass number of incident ion and target atom, E_d is the minimum displacement energy and R_c is the mean range of a displaced atom taken to be 1 nm [18]. Recently, Johnson *et al.* [19] derived a phenomenological expression for the effective mixing efficiency in the thermal spike region

$$\eta = \frac{K_1 S_n^2}{\rho^{5/3}\Delta H_{coh}^2}\left(1 + K_2\frac{\Delta H_m}{\Delta H_{coh}}\right) \tag{4}$$

where ρ is the average atomic density, ΔH_{coh} is the cohesive energy, and K_1 and K_2 are fitting constants with values of $K_1 = 0.0035$ nm and $K_2 = 27$.

When the mixing process of a constituent of a bilayered system arises due to a cascade mixing mechanism only, the mixing efficiency of the constituent should be proportional to the value of $S_n\xi_{21}/NE_d$ as shown in Equation 3, and it should be independent of ΔH_m. When the mixing process is induced by the thermal spike effect, the mixing efficiency should have a close relation with ΔH_m. Fig. 5c shows the mixing efficiencies of heavy elements, η_H, in binary systems as a function of $S_n\xi_{21}/NE_d$. η_H is proportional to the value of $S_n\xi_{21}/NE_d$ as expected from Equation 3, except for the Al–Cr system. The value of η_H for the Al–Cr system is considerably larger than the expected value from Equation 3. Some of the Al–Cr samples
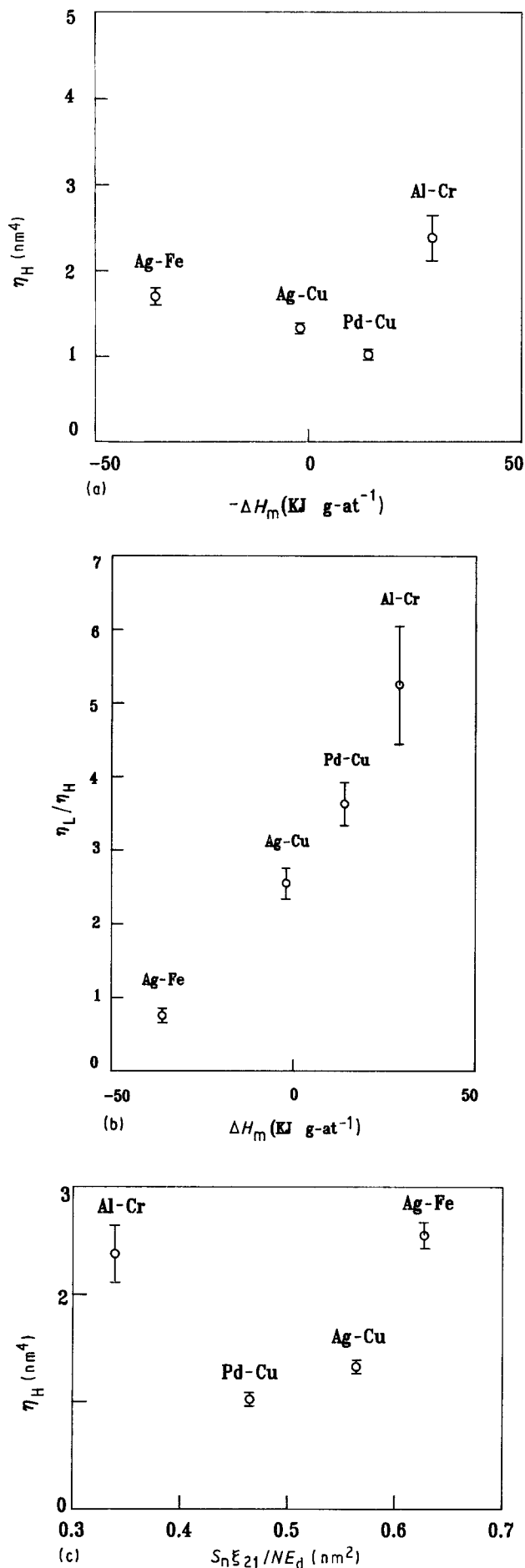
were studied by scanning electron microscopy. After irradiation with 1×10^{16} Ar^+ cm^{-2}, the surface of the Al layer has a dense distribution of 0.1–0.2 μm size craters, which would cause an anomalously large degree of mixing in RBS analysis. Therefore we suggest that the unexpectedly larger value of η_H for the Al–Cr system might be due to the dense distribution of craters.

Thus we conclude that the mixing mechanism for the heavier elements in a bilayered system is due to the cascade mixing process, and lighter elements are inter-diffused by thermal spike-induced mixing.

In terms of the ion-beam mixing model mentioned above, this suggests the following. Assuming that the value of R_c^2/E_d for the light element is approximately equal to the value for the heavy element in a binary system, the relocation of heavier atoms in the light-element side is favoured against the relocation of lighter atoms in the heavy-element side because the nuclear energy deposition in the heavy-element side is about 2–3 times higher than in the light-element side. Therefore the light element interdiffuses faster than the heavy element, and the heavy element may lose a chance to reach the thermal-spike mixing phase. Thus the heavy element interdiffuses by cascade mixing as shown in Fig. 5a and c, while the light element interdiffuses due to the thermal spike-induced mixing as shown in Fig. 5b.

4. Conclusion

Ar^+ ion beam-induced mixing of Al–Pd, Al–Cr, Pd–Cu, Ag–Cu and Ag–Fe bilayers has been studied using RBS and AES techniques for ion doses in the range between 1×10^{15} and 1×10^{16} Ar^+ ions cm^{-2} at room temperature. The mixing-induced AES depth profile at the Al–Pd interface deviated significantly from the Gaussian error function. Therefore, the mixing efficiencies of Al and Pd atoms are evaluated as a function of depth by the Boltzmann–Matano method. The mixing efficiencies are found to be far from constant and show maxima near the Al–Pd interface. The maximum value of the mixing efficiency for Al is higher than that of Pd by a factor of 4. This profile of mixing efficiency is very similar to the nuclear energy deposition profile. Also, the average mixing efficiencies in the Al–Cr, Pd–Cu, Ag–Cu and Ag–Fe systems from RBS analysis reveal that the mixing efficiencies of heavy elements (Cr, Pd, and Ag) are independent of the heat of mixing energy or migration enthalpy, while those of light elements (Al, Cu and Fe) have a close relationship with the heat of mixing energy, which means that in a binary system, the heavy element interdiffuses by the cascade mixing mechanism and the light element interdiffuses due to the thermal-spike mixing mechanism associated with damage-controlled diffusion.

Figure 5 (a) Mixing efficiencies of the heavy elements, η_H. (b) Ratio of mixing efficiencies of the light element, η_L, to that of the heavy element, η_H, as a function of ΔH_m. (c) Mixing efficiencies of the heavy elements, η_H, as a function of $S_n \xi_{21}/NE_d$ in Ag–Fe, Ag–Cu, Pd–Cu and Al–Cr binary systems.

2145

References

1. B. X. LIU, *Phys. Status Solidi (a)* **94** (1986) 11.
2. W. XIA, M. FERNANDES, C. A. HEWETT, S. S. LAU, D. B. POKER and J. P. BIERSACK, *Nucl. Instrum. Meth.* **B37/38** (1988) 408.
3. B. RAUSCHENBACH, M. POSSERT and R. KUCHLER, *Appl. Phys.* **A48** (1987) 347.
4. K. TAO, C. A. HEWETT, S. S. LAU, Ch. BUCHAL and D. B. POKER, *Appl. Phys. Lett.* **50** (1987) 1343.
5. R. J. SMITH, C. N. WHANG, XU MINGDE, M. WORTHINGTON, C. HENNESSEY, M. KIM and M. HOLLAND, *Rev. Sci. Instrum.* **58** (1987) 2284.
6. L. R. DOOLITLE, *Nucl. Instrum. Meth.* **B15** (1986) 227.
7. S. HOFMANN, in "Practical Surface Analysis by Auger and X-ray Photoelectron Spectroscopy", edited by D. Briggs and M. P. Seah (Wiley, Chichester, 1983) p. 141.
8. P. G. SHEWMON, in "Diffusion in Solids" (McGraw-Hill, New York, 1963) Ch. 1.
9. D. PEAK and R. S. AVERBACK, *Nucl. Instrum. Meth.* **B7/8** (1985) 561.
10. B. M. PAINE and R. S. AVERBACK, *ibid.* **B7/8** (1985) 666.
11. M. W. GUINAN and J. H. KINNEY, *J. Nucl. Mater.* **103/104** (1981) 1319.
12. J. P. BIERSACK, *Nucl. Instrum. Meth.* **B19/20** (1987) 32.
13. J. F. ZIEGLER, J. P. BIERSACK and U. LITTMARK, "The Stopping and Range of Ions in Solids" (Pergamon, New York. 1985).
14. K. HOHMUTH, V. HEERA and B. RAUSCHENBACH, *Nucl. Instrum. Meth.* **B39** (1989) 136.
15. A. D. MARWICH, in "Surface Modification and Alloying", edited by J. M. Poate, G. Foti and D. C. Jacobson (Plenum, New York 1983) p. 199.
16. R. HULTGREN, in "Selected Values of the Thermodynamic Properties of Binary Alloys" (American Society for Metals, Ohio, 1973) p. 199.
17. P. SIGMUND and A. GRAS-MARTI, *Nucl. Instrum. Meth.* **182/183** (1981) 25.
18. H. H. ANDERSEN, *Appl. Phys.* **48** (1979) 3383.
19. W. L. JOHNSON, Y. T. CHENG, M-van ROSSUM and M. A. NICOLET, *Nucl. Instrum. Meth.* **B7/8** (1985) 657.